LANGMUIR

pubs.acs.org/Langmuir Article

# Nanoparticle-Based Tough Polymers with Crack-Propagation Resistance

Yuma Sasaki, Yuichiro Nishizawa, Takumi Watanabe, Takuma Kureha, Kazuya Uenishi, Kazuko Nakazono, Toshikazu Takata,* and Daisuke Suzuki*

Cite This: *Langmuir* 2023, 39, 9262–9272 Read Online

ACCESS | Metrics & More | Article Recommendations | Supporting Information

**ABSTRACT:** Although thin elastomer films of polymer nanoparticles are regarded as environmentally friendly materials, the low mechanical strength of the films limits their use in various applications. In the present study, we investigated the fracture resistance of latex films composed of acrylic nanoparticles where a small quantity of a rotaxane crosslinker was introduced. In contrast to conventional nanoparticle-based elastomers, the latex films composed of the rotaxane-crosslinked nanoparticles exhibited unusual crack propagation behavior; the direction of crack propagation changed from a direction parallel to the crack to one perpendicular to the crack, resulting in an increase in tear resistance. These findings will help to broaden the scope of design of new types of tough polymers composed of environmentally friendly polymer nanoparticles.

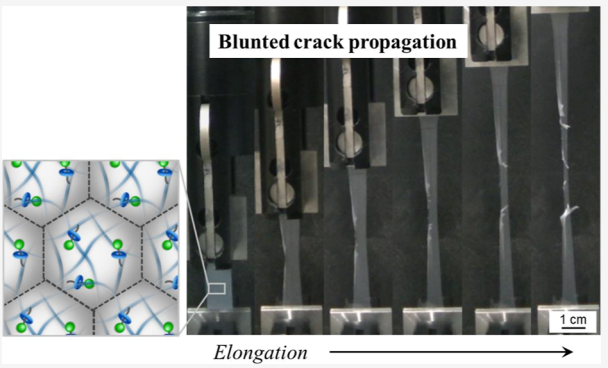


## INTRODUCTION

Polymer nanoparticles, with diameters that usually range from the submicron level to several microns, dispersed in water are widely used materials because of their fascinating properties, such as their large specific surface area, high colloidal stability, and uniform properties and size.[1−5] Therefore, there has been much fundamental research conducted on polymeric nanoparticles and their various potential applications as functional materials in biomedicine, energy, and electronics.[1,3,6−9] Polymer nanoparticles are used not only as single nanoparticles but also as assemblies. For instance, nanoparticle assemblies, known as colloidal crystals,[10−14] exhibit unique optical properties and respond rapidly to environmental changes.[15,16]

It is well known that synthetic polymer latexes, i.e., polymer nanoparticles dispersed in aqueous solution, form a continuous thin film upon evaporation of water.[17,18] Waterborne latex films, which do not contain volatile organic compounds, are regarded as environmentally friendly alternatives to polymer films based on organic solvents. Generally, latex films are formed when the solvent evaporates from the dispersion and the nanoparticles are packed as the drying proceeds.[17,18] The nanoparticles deform if the glass transition temperature ($T_g$) of their constituent polymers is lower than the drying temperature. Finally, the interdiffusion of polymer chains at the boundaries of the nanoparticles occurs, resulting in the formation of a coherent film. Latex films that readily form films and are easily processed have been used in many applications, for instance, in the coatings industry.[19−21] However, latex films formed by simple drying of water are known to be mechanically generally weak.[22−25] Thus, much effort has been expended to improve the mechanical properties of latex films. For instance, plasticizers are effective for decreasing the minimum film formation temperature (MFFT), resulting in cohesive and mechanically stable films.[26] Fillers (e.g., silica or other inorganic particles) are also used to enhance the elastic modulus and toughness of latex films through a composite effect.[27,28] Multiphase nanoparticles (i.e., core−shell structures) with a hard phase composed of a polymer with a high $T_g$ to improve the mechanical strength, and a soft phase composed of polymer with a low $T_g$ to aid the interdiffusion of the polymer chains, have also been utilized.[23,29,30] In addition, the strengthening of the interactions at the interparticle boundaries via chemical bonding[31−34] or hydrogen bonding[35,36] has been reported to be an effective way to obtain hard latex films. In these methods, reactive functional groups are introduced onto the surface of the nanoparticles and a chemical reaction proceeds to form a chemical crosslink between the nanoparticles.

In this context, our group has reported toughened latex films that utilize nanoparticles crosslinked with a rotaxane.[37−39] Compared with conventional latex films, latex films composed

Received: May 8, 2023
Revised: June 6, 2023
Published: June 16, 2023






https://doi.org/10.1021/acs.langmuir.3c01226
*Langmuir* 2023, 39, 9262−9272

Table 1. Chemical Composition, $D_h$ Acquired from DLS, and Swelling Ratio, $\alpha$, Calculated from eq 4 for the EM and EM-R*X* Nanoparticles Used in This Study[a]

| | monomers/crosslinker | | | | | |
|---|---|---|---|---|---|---|
| code | EA / mol % | MMA / mol % | RC / mol % | $D_h$ in water / nm | $D_h$ in DMF / nm | swelling ratio $\alpha$ |
| EM | 65.0 (3.75 g) | 35.0 (2.02 g) | 0 | 77 ± 0.3 | N.A. | N.A. |
| EM-R0.001 | 65.0 (3.75 g) | 35.0 (2.02 g) | 0.001 (0.001 g) | 100 ± 0.2 | 373 ± 4.6 | 51.5 |
| EM-R0.01 | 65.0 (3.75 g) | 35.0 (2.02 g) | 0.01 (0.007 g) | 82 ± 0.7 | 300 ± 0.2 | 49.3 |
| EM-R0.02 | 65.0 (3.75 g) | 35.0 (2.02 g) | 0.02 (0.013 g) | 90 ± 0.2 | 298 ± 0.7 | 36.4 |
| EM-R0.05 | 65.0 (3.75 g) | 35.0 (2.02 g) | 0.05 (0.033 g) | 106 ± 0.4 | 336 ± 2.0 | 31.8 |
| EM-R0.2 | 64.9 (3.74 g) | 34.9 (2.01 g) | 0.2 (0.130 g) | 100 ± 0.6 | 273 ± 1.6 | 20.0 |
| EM-R0.4 | 64.7 (1.87 g) | 34.8 (1.01 g) | 0.4 (0.13 g) | 85 ± 0.2 | 200 ± 0.4 | 13.1 |

[a]Note that $D_h$ for EM-R0.001 and EM-R0.01 in DMF were calculated excluding small size components.

of rotaxane cross-linked polymer nanoparticles have, as revealed by tensile tests, higher elongation and fracture energies.[37] Our studies differ from earlier works related to soft materials containing (poly)rotaxanes,[40−43] in that a small amount of the rotaxane is introduced into a single nanoparticle as a crosslinker.[37] Moreover, as revealed using small angle X-ray scattering (SAXS), the toughness of nanoparticle films cross-linked with a rotaxane crosslinker (RC) was enhanced using thermal annealing due to the acceleration of the interpenetration between the polymers at the surface of the polymer nanoparticles.[38,39] Our results indicate that the utilization of RCs in a nanoparticle is useful not only for increasing the mechanical strength of latex films but also for reducing any additives that are usually mixed in the latex films. However, it is still unknown how and why latex films are toughened when a RC is introduced into a single nanoparticle.

In the present study, we investigate the unique mechanical properties of tough nanoparticle-based polymers via the study of the tearing and tensile deformation of acrylate-based latex films. It is widely accepted that the tear test enables the understanding of the mechanical properties of materials in more detail via the use of notched specimens, and, thus, the tear test is one of the most reliable methods to evaluate the toughness of elastic materials[44,45] and even biological tissues.[46] The analysis of crack propagation resistance gives an insight into the network structure and toughening mechanism of materials.[47] Through a series of investigations, the effects of rotaxane crosslinking on toughed latex films is discussed.

## EXPERIMENTAL DETAILS

**Materials.** Ethyl acrylate (EA, >97.0%), methyl methacrylate (MMA, >98.0%), potassium peroxodisulfate (KPS, 95%), 1,6-hexanediol dimethacrylate (HDD, >98%), *N*,*N*-dimethylformamide (DMF, >99.5%), and ethanol (99.5%) were purchased from FUJIFILM Wako Pure Chemical Corporation (Japan) and used as received. Sodium dodecylbenzenesulfonate (DBS, >95.0%) and hexadecane (HD, >99.5%) were purchased from Tokyo Chemical Industry Co., Ltd. (Japan) and used as received. Deionized water was prepared using an EYELA, SA-2100E1 (Japan). The synthesis of the RC is described elsewhere.[48]

**Preparation of Elastomer Nanoparticles via Mini-Emulsion Polymerization.** Non-crosslinked poly(EA-*co*-MMA) (denoted as EM) and rotaxane-crosslinked EM-R*X* nanoparticles, where *X* signifies the RC feed ratio (*X* = 0.001, 0.01, 0.02, 0.05, 0.2, 0.4), were synthesized via mini-emulsion polymerization performed in an aqueous medium.[49] The monomer solution of EA, the MMA crosslinker (HDD or RC) in the quantities listed in Table 1, and HD (0.46 g) were poured into a surfactant-water solution (DBS 0.10 g, water 30 g). Next, the water and monomer suspension was homogenized using ultrasonication (VCX-750, Ieda Trading Corporation, Japan) with an output of 375 W for 3 min to form an oil in water emulsion. The emulsion was added into a three-neck round-bottom flask (50 mL) with a stirrer, a condenser, and nitrogen gas inlet fitted. Then, the emulsion was heated to 70 °C using an oil bath. After bubbling with nitrogen gas for 30 min, this was changed and the nitrogen gas was allowed to flow over the emulsion. KPS (0.10 g) was dissolved in 6 mL of water and was added to the emulsion, and the polymerization was initiated. After 4 h, the dispersions were cooled with an ice bath to terminate the polymerization. The dispersions were purified via centrifugation at 15 °C (relative centrifugal force = 20,000*g*; ∼30 min, 2 cycle) and redispersed in water, followed by dialysis (1 week, the water was changed daily) to remove impurities including surfactants, excess initiator, and free polymer chains.

**Nanoparticle Characterization.** The morphology of the nanoparticles was evaluated by atomic force microscopy (AFM, AFM5200S, Hitachi High-Tech Corporation, Japan) using an SI-DF20 microcantilever (spring constant: 15 N/m, tip diameter: 20 nm, Hitachi High-Tech Corporation, Japan). The nanoparticle dispersion (0.1 wt %) was mixed with the same volume of ethanol and then the dispersions of water/ethanol (200 $\mu$L) were spread onto the air/water interface of a $\varphi$5 cm glass Petri dish (depth; ∼1 cm). After allowing to stand for 1 min, a glass substrate (18 mm × 18 mm; Matsunami Glass Ind., Ltd., Japan) was raised in a direction vertical to the air/water interface. The glass substrate was washed with detergent and deionized water prior to use in the measurements. The height and full width at half maximum (FWHM) of the nanoparticles were analyzed using a NanoNavi Station (Hitachi High-20 Tech Science Corp.).

For the evaluation of the nanoparticle width of individual pEM nanoparticles, transmission electron microscopy (TEM) was used (JEOL2010, Japan; acceleration voltage: 80 kV). For the TEM observations, nanoparticles were spread at the air/water interface using the same method as for the AFM measurements (vide supra). The supporting substrate (copper grid, Sheet Mesh 150-A Cu, Nisshin-EM, Japan) was raised in a direction perpendicular to the air/water interface in order to select the nanoparticles. The width of the nanoparticles was analyzed using ImageJ software (version 1.53t; Wayne Rasband, National Institutes of Health, USA).

The hydrodynamic diameter ($D_h$) was determined using dynamic light scattering (DLS, Malvern Instruments Ltd., Zetasizer Nano S, UK). For the DLS measurements, dilute dispersions (nanoparticles 0.01 wt %) of 1 mL were prepared. To reach thermal equilibration at 25 °C, the sample was left to stand for 600 s prior to the DLS measurements. The correlation function of the scattering intensity $g_2(\tau)$ is given by eq 1, where $g_1(\tau)$ is the correlation function of the scattering electric field, $\beta$ is the extrapolated value at $\tau$ = 0.

$$g_2(\tau) - 1 = \beta |g_1(\tau)|^2 \quad (1)$$

Here, $g_1(\tau)$ is provided by eq 2, where $D$ is the diffusion coefficient, and $q$ is the scattering vector [$=(4\pi/\lambda)\sin(\theta/2)$] ($\lambda$ = 633 nm, $\theta$ = 173°).

$$g_1(\tau) = \exp(-Dq^2t) \quad (2)$$



https://doi.org/10.1021/acs.langmuir.3c01226
Langmuir 2023, 39, 9262−9272

The hydrodynamic diameter, $D_h$, was calculated using the Stokes−Einstein equation, where $k$ is the Boltzmann constant and $T$ is the absolute temperature (298 K), while $\eta$ is the viscosity of water at 298 K.

$$D_h = kT/3\pi\eta D \quad (3)$$

The $D_h$ was calculated from the cumulant analysis of the correlation function, where diffusion coefficients were evaluated using the Stokes−Einstein equation (Zetasizer software v6.12) based on the average of three cycles of measurements (30 s). The swelling ratio $\alpha$ was defined as follows.

$$\alpha = (D_{h\ in\ DMF}/D_{h\ in\ water})^3 \quad (4)$$

The gel content (GC %) of the nanoparticle was determined using Soxhlet extraction.[23] For that purpose, toluene was selected as a solvent to dissolve the nanoparticles. Prior to the extraction, the latex was dried at 25 °C on a PTFE sheet (TOMBO No. 9001). After the extraction was carried out for 12 h, the solvent was removed from the extraction residue (soluble fraction) under reduced pressure, followed by drying in air (3 days). The GC % was defined as follows, where $w_1$, $w_2$ represents the insoluble mass and original mass of polymer, respectively.

$$GC\% = (w_1/w_2) \times 100 \quad (5)$$

For measurements of the molecular weight of the EM nanoparticles using gel-permeation chromatography (GPC), the soluble fraction of the Soxhlet extraction was dried at 25 °C for 24 h, and then redissolved in DMF. The solution (~2.5 mg/mL) was filtered (Minisart SRP Syringe Filter, $\phi$ = 15 mm, pore size: 0.2 $\mu$m) prior to the injection. GPC measurements were performed using the following conditions: GPC KD-805 column (Shodex, Japan), DMF (flow: 1 mL/min), 40 °C. Molecular weights were calculated using a calibration curve obtained from polymethyl methacrylate standards.

The thermal properties of the nanoparticles were evaluated from differential scanning calorimetry (DSC, DSC-60, Shimadzu Corporation, Japan) measurements. The dispersions were freeze-dried (FDU-1200, Tokyo Rikakikai Co., Ltd., Japan) to completely remove water from the samples. The dried nanoparticles (25 mg) were packed into an aluminum pan. Alumina powder (50 mg) was also packed into the aluminum pan as a reference. The nanoparticles and alumina in the pan were set in a chamber under a flow of nitrogen gas (60 mL/min). The sample was heated from −110 to 120 °C at a rate of 10 °C/min.

**Tensile Tests of the Latex Films.** To prepare the tensile test specimens from the poly(EA-*co*-MMA) nanoparticles, a dispersion (~8 wt %) containing 24 mg nanoparticles was poured into a dumbbell-shaped mold (ISO37-4) made from silicone rubber, which allows picking up films without causing any damage, and then dried for 24 h at 25 °C in a low temperature incubator (LTI-2100, EYELA, Japan). The tensile tests were performed using an STB-1225L (A&D Co., Ltd., Japan) with a 50 N load cell at a stretching rate of 10 mm/min. The measurements were performed at 23 ± 1 °C.

**Tear Tests of the Latex Films.** For the preparation of the tear test specimens, 175 mg nanoparticle dispersions were poured into a square-shaped mold (3.5 cm × 3.5 cm) made from silicone rubber and then dried at room temperature. The obtained films formed by casting of the dispersions were cut to a size of 1 cm × 3.5 cm using a scalpel (Figure S1). Each sample was measured more than three times and the stress−strain and stress-extension ratio curves were plotted for the sample closest to the average. The tensile tester used in the tear tests is the same as the tensile test described above. The distance between the attachments was 20 mm. Each measurement was performed at 23 ± 1 °C. For evaluation of the fracture toughness, a 2 mm precut is inserted at the center of one side of the film.[50] The elongation rates were 1, 10, 30, 50, 80, 100, and 500 mm/min. Experimentally, the input energy for complete fracture including blunted crack propagation $W_{tear}$ was defined as the integration of $\sigma-\lambda$ curves until complete fracture (eq 6). The $\lambda_{max}$ was defined as the maximum extension ratio when films were completely fractured.

$$W_{tear} = \int_1^{\lambda_{max}} \sigma(\lambda) d\lambda \quad (6)$$

**Film Surface Characterization.** The surfaces of the latex films were characterized using scanning electron microscopy (SEM, JEOL Ltd., JCM-7000). Prior to observation, the films were sputtered with Pt/Pd (15 mA, 6 Pa, 30 mm distance from the films for 80 s).

**SAXS Measurements and Analysis.** The nanostructures of the latex films were characterized using SAXS at the BL03XU beamline of SPring-8 (Hyogo, Japan). The wavelength and beam size of the X-rays were 0.10 nm and 50 $\mu$m × 50 $\mu$m, respectively. The sample-to-detector distance (camera length) was 4.0 m. The tested latex films were attached to the sample holder and the exposure time was 15 s. The obtained two-dimensional images were circularly integrated using FIT2D to obtain 1D scattering profiles. The film dimensions for the SAXS measurements were 10 mm × 10 mm × 1 mm squares. The interfacial thickness ($t_{inter}$), which is an indicator of interpenetration depth, was calculated based on Porod's law by analyzing the deviation of the SAXS intensity in the high scattering-vector ($q$) range as follows:

$$I(q) = Cq^{-4} \exp(-\sigma^2 q^2) \quad (7)$$

where $C$ is a constant and $\sigma$ represents the diffuseness of the boundary. In this method, the thickness of the domain boundaries in the block-copolymer systems, where the block-copolymers with different electron density form the domain structures (denoted here as a "pseudo-two-phase system") was applied to the nanoparticle films.[51−53] For the analysis, it was assumed that two different electron densities exist in the nanoparticle film. In particular, the nanoparticle core has a low-density matrix, while the mixing area between the charged groups, localized at the nanoparticle surface, is characterized by high density. In other words, the delocalization of charged groups, i.e., the diffusion of sulfonate acids occurred upon mixing surface-near polymer chains on the microspheres during film formation.[39,54,55] In order to calculate the interfacial thickness according to Ruland's theory for two-phase materials with diffuse boundaries,[56] the electron-density variation of the pseudo-two-phase system along the normal, $\eta(z)$, is followed by a convolution product of a step function, $g(z)$, and a Gaussian smoothing function, $h(z)$ as follows:

$$\eta(z) = g(z) \cdot h(z) \quad (8)$$

$$h(z) = (2\pi\sigma^2)^{-1/2} \exp(-z^2/2\sigma^2) \quad (9)$$

In this study, the background scattering arising from the thermal density fluctuation from the total scattered intensity was subtracted from the SAXS intensity, $I(q)$, by assuming that the background scattering is given by a straight line, which is the intensity of the highest observed $q$ values (0.09 Å$^{-1}$). It should be noted here that this is purely an empirical procedure and that there is also a way to subtract a curved background scattering. However, our manner of subtracting the background scattering did not significantly affect the value of $\sigma$ or $t_{inter}$ (the difference was <10%). In brief, a plot of the scattered intensity $I(q)$ as a function of $q^2$ affords a straight line. When the obtained slope, which represents the value of $\sigma$, is negative, it means that a scattering contribution from the interfacial thickness exists in the film. The interfacial thickness ($t_{inter}$) is, thus, given by the following equation:[39]

$$t_{inter} = (2\pi)^{1/2}\sigma \quad (10)$$

## RESULTS AND DISCUSSION

**Preparation and Characterization of the Nanoparticles.** To obtain free-standing films via the evaporation of water from the dispersion under ambient conditions, MMA, of which polymer (polyMMA) has a higher glass transition temperature ($T_g$ ~ 100 °C),[57] was copolymerized with EA to control the nanoparticle $T_g$ (Figure 1a).[17,54] Here, the RCs, which have one axle penetrating one wheel and have a


https://doi.org/10.1021/acs.langmuir.3c01226
Langmuir 2023, 39, 9262−9272

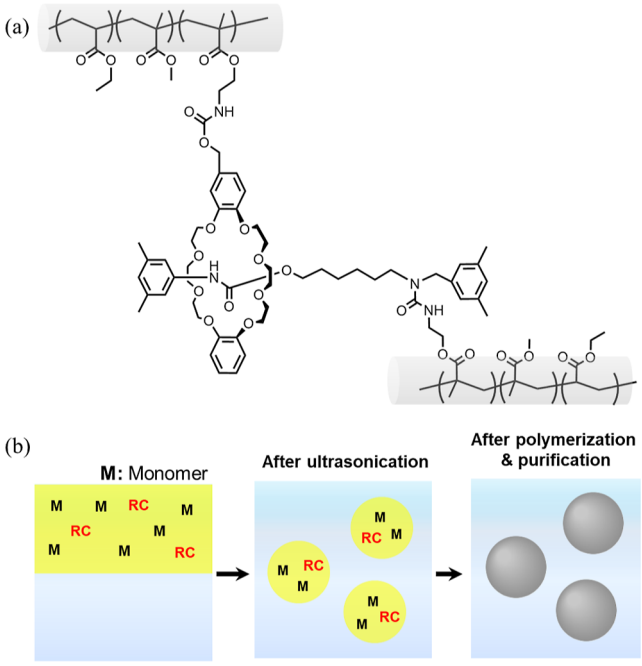


**Figure 1.** (a) The chemical composition of the EM-R*X* nanoparticles crosslinked with the RC used in this study. (b) Schematic illustration of the nanoparticle synthesis using a mini-emulsion polymerization method.

polymerizable functional group on each axle and wheel component, were selected for the polymerization in order to control the degree of crosslinking that occurs in a single nanoparticle (Figure 1a).[37] To efficiently incorporate the water immiscible RCs into the individual nanoparticles, mini-emulsion polymerization was utilized, where ideally a single oil droplet becomes a single polymer nanoparticle (Figure 1b).[37,49] In this case, the amount of RC fed into the reaction vessel during the polymerization was systematically changed from 0.001 to 0.4 mol % allowing us to clarify the effect that rotaxane crosslinking has on a single nanoparticle, and, thus, on the mechanical properties of their latex films (Table 1). It should be noted here that the copolymerization ratios of EA and MMA were selected as 65/35 (mol %/mol %) since their $T_g$ is ∼9 °C (as determined by DSC; Figure S2). Here, given that the MFFT of nanoparticles is likely to be below the $T_g$ by water acting as a plasticizer,[17,18] these nanoparticles fully undergo deformation and film formation at room temperature. Generally, the MFFT of nanoparticles is close to their $T_g$.[17,18] Thus, these nanoparticles enabled us to make free-standing nanoparticle-based films under ambient conditions (i.e., ∼25 °C). DSC curves of the EM nanoparticles showed that a heat-flow change was observed only at ∼10 °C, which confirmed that a phase-separation does not occur, given that clearly phase-separated nanoparticles show two glass-transition peaks originating from polyEA and polyMMA, respectively.[30]

As can be seen from the AFM and TEM images, the series of EM and EM-R*X* nanoparticles were uniform in size (coefficient of variation <11%), and their diameters were estimated from the FWHM to be ca. 100 nm, which was close to that obtained by TEM (Figure 2a, Figures S3 and S4). In addition, the EM nanoparticles were not aggregated, as was clearly confirmed by the non-closed packing arrangement of the nanoparticle structures formed when using an air/water interface as the arrangement site.[58] Next, to confirm that the RC had been incorporated into the individual EM nanoparticles, the swelling ratio $\alpha$ was calculated, according to eq 4 (Table 1), from the hydrodynamic diameters ($D_h$) in water divided by the $D_h$ in a good solvent (DMF). In all cases, the $D_h$ in water is ∼100 nm, which is similar to the value estimated from the AFM analysis (Figure S3). There is a clear tendency for $\alpha$ to decrease as the amount of RC fed into the reaction increases during the polymerization, indicating that the RC was successfully introduced into the nanoparticles in a controlled manner. It was also confirmed that the gel content (GC %) of the nanoparticle obtained from Soxhlet extraction increases with the amount of rotaxane (EM: <1%, EM-R0.001: <1%, EM-R0.01: 3%, EM-R0.02: 5%, EM-R0.05: 20%, EM-R0.2: 38%, Figure S5a). The molecular weight of the soluble fraction of the EM acquired from GPC ($M_n$ = 3.05 × $10^5$ g/mol, $M_w$ = 8.72 × $10^5$ g/mol; Figure S5b) was close to that of the polyacrylate nanoparticles synthesized via the emulsion polymerization in the previous study.[59]

**Preparation and Characterization of the Latex Films.** Latex films were prepared by drying the nanoparticle dispersions at 25 °C for 24 h (Figure S1). In all cases, the quantity of nanoparticles was fixed (175 mg for 3.5 cm × 3.5 cm) and the thickness of the films was controlled to be ∼0.15 mm. In this study, free-standing latex films were obtained when the degree of RC crosslinking was lower than 0.2 mol %. Nanoparticles with a higher degree of RC crosslinking (i.e., EM-R0.4) formed brittle films that were unsuitable for the mechanical tests due to the decreased deformability of the nanoparticles (Figure S6). This presumably occurs because the highly crosslinked nanoparticles could not be deformed during the film formation process, even though movable RCs were used.

Homogeneous films without wrinkles or uneven coloration were obtained, and their appearance, as confirmed via visual observation, did not change, regardless of the amount of RC introduced into the nanoparticles (Figures 2b and S7a). SEM observation of the surface of the latex films also revealed that there are no remarkable microscopic structural defects. The nanoparticles were found to be densely packed and highly deformed in the films (Figures 2c and S7b), and, thus, the individual nanoparticles could not be distinguished.

**Crack Propagation Resistance of the Latex Films.** Mechanical tests were performed on the latex films (Figure 2d). The elongation rate was fixed at 10 mm/min in all cases. Video and photograph snapshots taken during a tear test of the non-crosslinked EM film show a normal crack propagation (Figure 2d, EM, Movie S1). The rate of crack propagation of EM-R0.001 and EM-R0.01 films was faster than that of EM films because the Young's modulus of EM-R0.001 and EM-R0.01 films was higher than that of EM films and the stress increased as the elongation proceeded (Figure 2d, Table 2). Conversely, the EM-R0.02 film underwent a blunted crack propagation at the latter stages of elongation. The direction of crack propagation changed from parallel to perpendicular to the crack, i.e., parallel to the direction of elongation (Figure 2d, EM-R0.02, Movie S2). Furthermore, we found that the blunted crack propagation behavior of the EM-R*X* films depends on the degree of crosslinking. Similar to the EM-R0.02 film, the EM-R0.05 and EM-R0.2 films also underwent blunted crack propagation with a higher degree of elongation reached before film fracture (Figure S8). In contrast, the EM-R*X* films with lower degrees of crosslinking ($X$ = 0.001, 0.01) did not exhibit the same crack propagation behavior, and, as seen with the EM


https://doi.org/10.1021/acs.langmuir.3c01226
Langmuir 2023, 39, 9262−9272

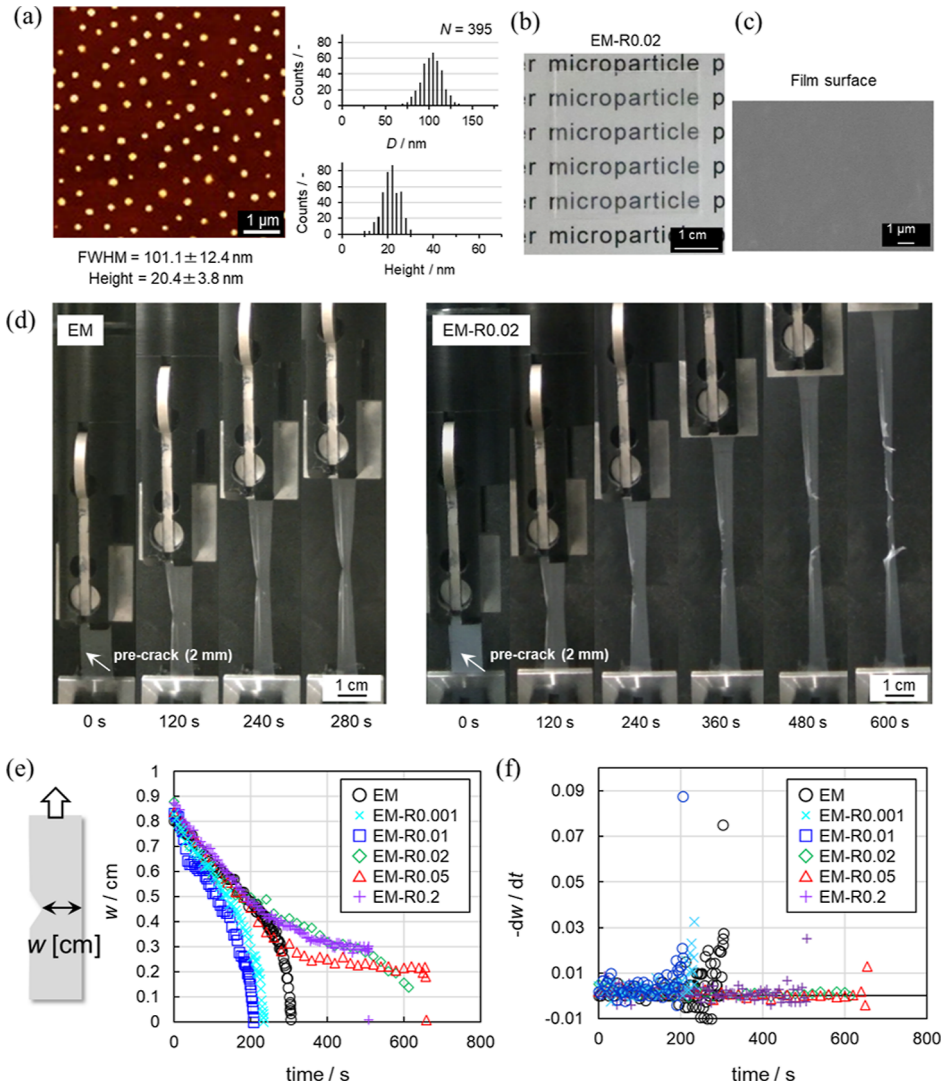


**Figure 2.** (a) AFM height image of the EM-R0.02 nanoparticles dried on a glass substrate and their determined sizes (FWHM and the maximum height). (b) Photograph and (c) SEM image (surface) of the EM-R0.02 films. (d) Photograph snapshots taken during the tear tests of the EM and EM-R0.02 films. The initial crack length was 2 mm and the elongation rate was fixed at 10 mm/min. (e) Film width $w$ and (f) $-dw/dt$ as a function of time.

**Table 2. Mechanical Properties' Parameters (Young's Modulus $E$, Input Energy for Complete Fracture, $W_{tear}$, Maximum Extension Ratio $\lambda_{max}$, and Maximum Stress $\sigma_{max}$) Obtained from Analysis of the $\sigma-\lambda$ Curves of the Latex Films**

| | Young's modulus $E$/MPa | energy for complete fracture $W_{tear}$/MJ m$^{-3}$ | maximum extension ratio $\lambda_{max}$/— | maximum stress $\sigma_{max}$/— |
|---|---|---|---|---|
| EM | 6.0 ± 2.9 | 1.7 ± 0.04 | 3.5 ± 0.04 | 0.8 ± 0.2 |
| EM-R0.001 | 9.0 ± 0.2 | 1.6 ± 0.5 | 2.7 ± 0.4 | 1.7 ± 0.7 |
| EM-R0.01 | 10.7 ± 4.1 | 2.2 ± 1.2 | 2.9 ± 0.7 | 1.7 ± 0.4 |
| EM-R0.02 | 12.0 ± 4.9 | 5.9 ± 3.0 | 4.7 ± 2.0 | 2.1 ± 0.1 |
| EM-R0.05 | 8.1 ± 1.4 | 52 ± 1.4 | 5.8 ± 0.7 | 2.1 ± 0.4 |
| EM-R0.2 | 12.2 ± 1.0 | 4.5 ± 0.04 | 5.0 ± 0.3 | 1.6 ± 0.04 |

film, conventional crack propagation was observed (Figure S8). The crack propagation rate ($-dw/dt$) of the films was evaluated from the change in the film width ($w$). In the case of EM and EM-R$X$ ($X$ = 0.001, 0.01) films, the crack propagation rate steeply increased after ~200 s due to the growth of the crack (Figure 2e,f). On the other hand, the $-dw/dt$ of the EM-R$X$ ($X$ = 0.02, 0.05, 0.2) films hardly changed until just before fracture (Figure 2e,f).

The stress-extension ratio ($\sigma-\lambda$) curves of the films revealed the maximum extension ratio ($\lambda_{max}$) and maximum stress ($\sigma_{max}$) for the EM-R0.02 (6.1, 1.7 MPa), EM-R0.05 (5.6, 1.7 MPa), and EM-R0.2 films (5.0, 1.2 MPa), the films that exhibit blunted crack propagation. The values obtained for these films were higher than those obtained for the EM (3.5, 0.7 MPa), EM-R0.001 (2.5, 1.4 MPa), and EM-R0.01 films (2.9, 1.3 MPa), the films that exhibit conventional crack propagation (Figure 3, Table 2). For the evaluation of the toughness of crack-propagation-blunted films, the input energy for complete fracture, $W_{tear}$, was estimated based on the sum of the $\sigma-\lambda$ curves using eq 6 (Table 2, Figure S9). In this study, the fracture energy based on Lake-Thomas theory was not defined because it was difficult to identify when the initial crack started to propagate (Figure S8). The EM-R0.02 film, a film that undergoes blunted crack propagation, has a significantly high $W_{tear}$ value of 5.9 MJ/m$^3$ because $\lambda_{max}$ is 6.1 and, thus, $\sigma_{max}$ is also 1.7 MPa (Table 2). In addition, the Young's moduli of


https://doi.org/10.1021/acs.langmuir.3c01226
Langmuir 2023, 39, 9262−9272

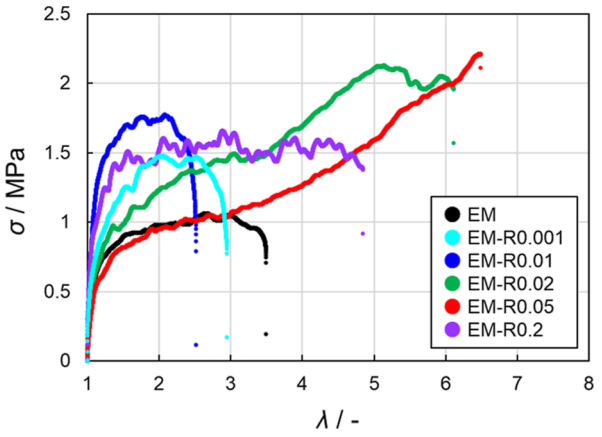


**Figure 3.** Stress ($\sigma$)-extension ratio ($\lambda$) curves for the tear tests of the EM and EM-R*X* latex films ($X$ = 0.001, 0.01, 0.02, 0.05, 0.2). The initial crack length was 2 mm and the elongation rate was fixed at 10 mm/min.

EM-R0.02 (6.8 MPa) and EM-R0.05 (6.4 MPa) were lower than those of EM-R0.001 (7.5 MPa) and EM-R0.01 (8.6 MPa), indicating stress dissipation resulting from the presence of the RCs (Table 2).[60,61]

Furthermore, the effect of conventional regular crosslinking using 1,6-hexanediol dimethacrylate (HDD) (Figure S10a), whose alkyl chain was the same length as the alkyl chain of rotaxane's axis was also investigated. It is confirmed that the blunted crack propagation was not observed at any elongation-rate when the regular and non-movable crosslinkers (HDD) were used (Figure S10b,c,d). These results indicated that the blunted crack propagation was observed only when the RCs were introduced into the nanoparticles.

**Microstructural Analysis of the Latex Films.** In order to clarify the microscopic structures of the films, SAXS was used. The SAXS profiles of the EM film revealed a Bragg peak originating from the face-centered-cubic (fcc) colloidal crystals in the low-$q$ range (Figure 4a).[62] However, the Bragg peak disappeared in the profiles of EM-R*X* ($X$ = 0.001, 0.01, 0.02, 0.05) as the degree of crosslinking increased. The Bragg peak appeared again when the degree of RC crosslinking was higher (i.e., the EM-R0.2 film). These results indicate that the EM-R0.001, -R0.01, -R0.02, and -R0.05 nanoparticles are highly deformed and coalesce with each other in the films. Next, the degree of interdiffusion between the nanoparticles was evaluated using Porod's law. The plots of [ln $q^4$ $I(q)$] as a function of $q^2$ for the tested films are displayed in Figure S11. According to eq 7, the slope was negative, suggesting that the interfacial thickness, i.e., mixing of polymers at the nanoparticle surface occurred in these films. The interfacial thickness ($t_{inter}$), which represents the degree of interdiffusion,[39] of the latex films increased as the degree of RC crosslinking increased up to 0.02 mol %. After this point, the $t_{inter}$ values of the EM-R0.05 and EM-R0.2 films were lower than those of the EM-R0.01 and EM-R0.02 films (Figure 4b). This result suggests that the cross-linked structures confined to the individual particles were replaced by diffused polymer chains that straddle the interface, resulting in the formation of a film with high mechanical strength. Conversely, excessive introduction of cross-linking into the interior of the particles would have reduced the number of chains involved in cross-linking on both sides of the interface, which would have resulted in decreased mechanical properties. Aradian et al. have concluded that the inter-penetration length decreases with increasing crosslinking density based on scaling arguments, which also supports these results.[63] This change suggests that the flexibility of the polymer chains was enhanced by the movable rotaxane crosslinking points when the appropriate amount of RC was introduced into the nanoparticles. It should be noted here that the interpenetration behavior of the nanoparticles has been investigated using small-angle neutron scattering (SANS), where the penetration depth was calculated by subtracting the original radius of the deuterated nanoparticles from the apparent radius of the deuterated nanoparticles.[64−66] Indeed, the obtained $t_{inter}$ values were close to the penetration depth (2−5 nm). In particular, the penetration depth contributed to the tensile strength of the polystyrene latex films when the depth was at least 3−3.5 nm.[66] The results of that SANS study are consistent with the results in this study, i.e., $t_{inter}$ of the EM-R0.2 films was <3.5 nm, and, thus, their fracture energy was lower than those of other rotaxane crosslinked nanoparticle films (Figure 4b). In addition, the $t_{inter}$ values correlate well with both the fracture energies of the notched tear tests and the unnotched tensile tests, indicating that the blunted crack

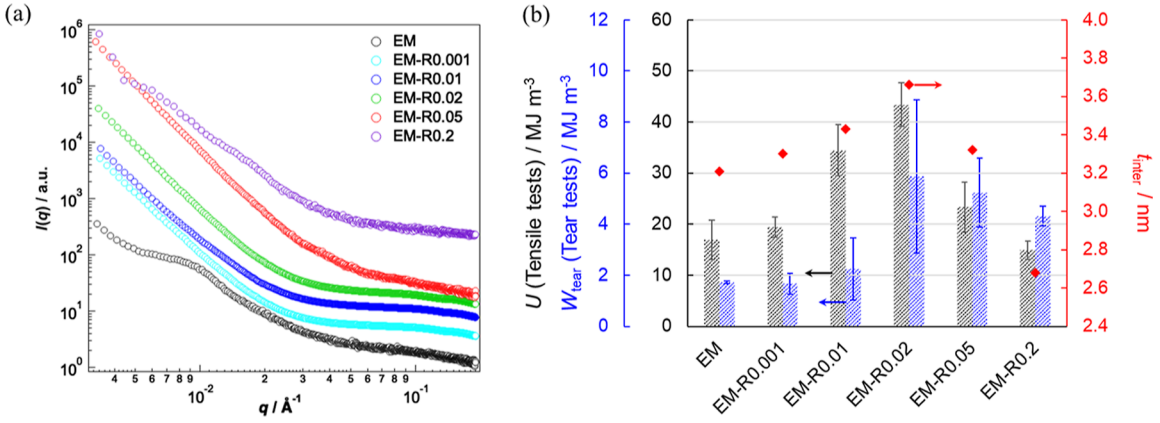


**Figure 4.** (a) SAXS profiles of the EM and EM-R*X* latex films. Each scattering intensity ($I(q)$) is vertically offset for clarity. (b) The correlation between the input energy for complete fracture, $W_{tear}$ obtained from the tear tests (notched samples, black bars) and the energy density function $U$ obtained from the tensile tests (unnotched samples, blue bar). The $t_{inter}$ values (red diamonds) calculated from the SAXS profiles using Porod's law are also shown.



https://doi.org/10.1021/acs.langmuir.3c01226
Langmuir 2023, 39, 9262−9272

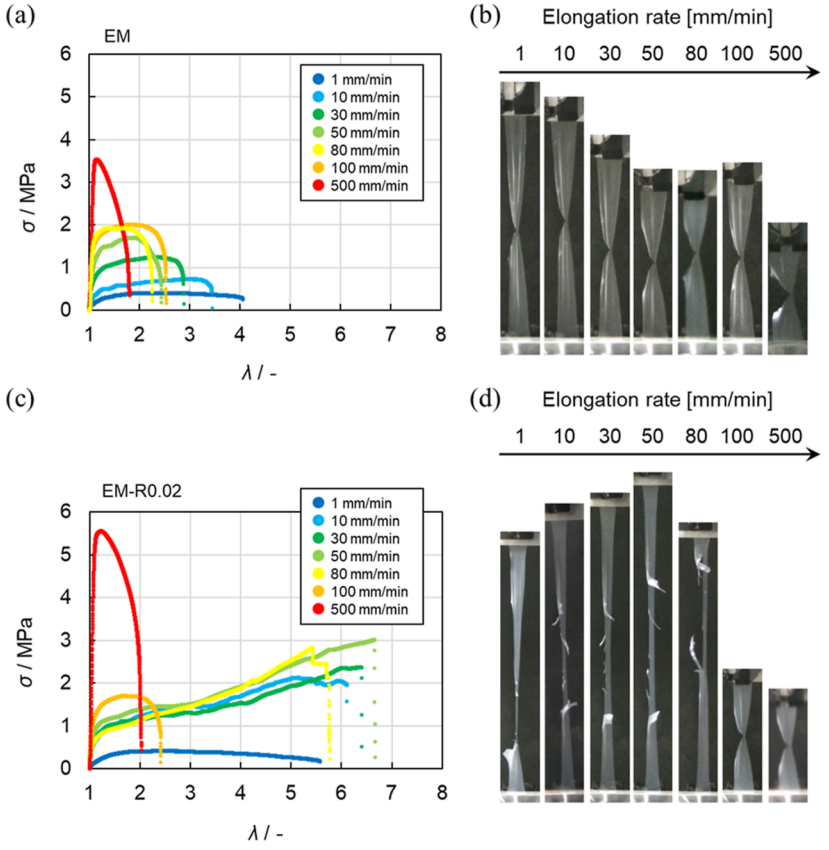


**Figure 5.** $\sigma$−$\lambda$ curves obtained from the tear tests of the (a) EM and (c) EM-R0.02 films measured at different elongation rates (1−500 mm/min). (b,d) Photographs of the latex films just before fracture at various elongation rates.

propagation is affected by the interpenetration depth between the nanoparticles in the films (Figures 4b and S12). The mechanical properties of the latex films depend on the interpenetration depth if the polymers are fully entangled.[66] Since the interfacial thickness ($t_{inter}$) of EM-R0.4 (3.04 nm) was lower than that of other rotaxane crosslinked nanoparticle films, it is indicated that the EM-R0.4 nanoparticles cannot fully be entangled between nanoparticles when the films were formed.

**Outcomes of the Tear Tests on the Latex Films at Different Elongation Rates.** The correlation between the deformation rate and the mechanical properties of many tough polymeric materials in tests that subject them to large deformations, such as tearing tests, has been investigated, and the toughening mechanism and the mechanics of these factors have been discussed.[50,67,68] To understand the dynamics of the RC in the nanoparticles during the tear test, we evaluated the mechanical properties at elongation rates ranging from 1 to 500 mm/min (Figure 5). The $\sigma$−$\lambda$ curves obtained at various elongation rates and the photograph snapshots taken just before fracture (i.e., $\lambda_{max}$) revealed that the $\sigma_{max}$ of the EM film during tearing increased as the elongation rate increased, while the value of $\lambda_{max}$ decreased (Figure 5a). Normal crack propagation was observed for the EM film at all elongation rates examined in this study (Figure 5b). However, in the case of the EM-R0.02 film, blunted crack propagation was observed and the $\lambda_{max}$ value remained almost unchanged at lower elongation rates (i.e., 1−80 mm/min) (Figure 5c). Conversely, at high elongation rates (100, 500 mm/min), blunted crack propagation was not observed and, in comparison with the values obtained at lower elongation rates, $\lambda_{max}$ dramatically decreased (Figure 5d).

In the case of a previously reported polyrotaxane hydrogel, it was found that the fracture energy evaluated in the tear test decreased at a deformation rate of more than 0.6 $s^{-1}$, indicating that the mobility of the rotaxane components could not keep up with the deformation of the material.[68] In the case of the EM-R$X$ ($X$ = 0.02, 0.05) latex films examined in this study, a transition between normal and blunted crack propagation was observed at rates of around 0.06−0.07 $s^{-1}$, which is a difference of an order of magnitude from the previous report on polyrotaxane hydrogels. This difference may be interpreted in light of the rotaxane environments; the rotaxane crosslinking points in elastomer latex films are more crowded than in the polymer chains of hydrogels, where polymer densities are much lower than those of elastomers.

Additionally, the relationship between the elongation rate and the fracture behavior of the films was also found to be related to the degree of crosslinking (Figure S13). The $\lambda_{max}$ of the EM-R0.02 film, which has polymer chains strongly interdiffused at the interface of the nanoparticles ($t_{inter}$ = 3.66 nm), was 5.6−6.7 at elongation rates of 1−80 mm/min. Under these conditions, blunted crack propagation was observed (Figure 6a). Similarly, the $\lambda_{max}$ of the EM-R0.05 film, with weaker interpenetration of the polymer chain ($t_{inter}$ = 3.32 nm) was 4.5−5.6, and blunted crack propagation was observed at elongation rates of 1−80 mm/min (Figure 6b and S13e,f). The $\lambda_{max}$ of the EM-R0.2 film ($t_{inter}$ = 2.68 nm) was 4.4−5.0, and the range of elongation rates where blunted crack propagation could be observed was narrower (1−30 mm/min) (Figures 6b and S13g,h). This narrower range indicates that


https://doi.org/10.1021/acs.langmuir.3c01226
Langmuir 2023, 39, 9262−9272

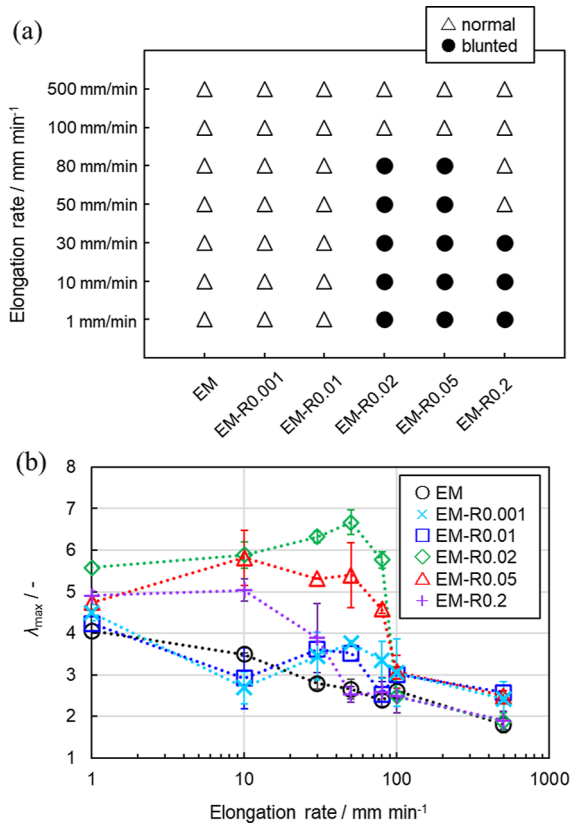


**Figure 6.** (a) Widths of the EM and EM-R*X* films during tear tests at different elongation rates (circle; blunted crack propagation; triangle; normal crack propagation). (b) $\lambda_{max}$ of the EM and EM-R*X* films at different elongation rates. Each value was plotted from the average of three measurements.

excess RCs constrain the mechanical properties of the latex films, as shown in our previous study on tensile tests.[37] As a result, it was confirmed that, at the same elongation rate (10, 30, 50, and 80 mm/min), $\lambda_{max}$ gradually decreases as the degree of crosslinking increases (Figure 6b). Taking all these data into account, it is clear that the reason why the latex films undergo blunted crack propagation is related to the presence of the RCs in the nanoparticles.

## DISCUSSION OF THE BLUNTED CRACK PROPAGATION OF THE LATEX FILMS

To date, reports on such an unusual form of crack propagation, blunted crack propagation, have been limited to cases of carbon black or silica-filled natural rubber[69,70] and flexible polymers with anisotropic structures formed from fillers[71] or fibers[72,73] or by microphase separation[74,75] or strain-induced crystallization.[76] In all cases, the anisotropic structures within the material change the direction of crack propagation, and, thus, they show high crack propagation resistance.

To the best of our knowledge, in the previous studies on the mechanical properties of latex films, there have not been any reports on the investigation of tear tests. In addition, there are a limited number of studies on the mechanical properties of latex films.[25−36] The novelty of our study is the excellent mechanical properties that arise from the use of a small amount of RC (e.g., 0.02−0.2 mol %) within a single nanoparticle. The rotaxane crosslinked nanoparticles enable us to obtain free-standing latex films via the simple evaporation of water without the use of any plasticizers or fillers. No anisotropic additives are used, and, thus, there is the possibility for the latex films to form anisotropic structures when they are elongated. The individual nanoparticles may play a role in creating an anisotropic structure as the rotaxane crosslinked nanoparticles can show large deformations, as has already been confirmed in other macroscopic rotaxane materials.[43] Furthermore, in our latex films, there are no chemical crosslinks between the nanoparticles, and the physical interpenetration between the nanoparticles has been quantitatively analyzed using X-ray scattering,[39] an area that has not been focused on in the polymer latex research field. In our tested specimens, there does not appear to be a physically connected interface between the nanoparticles. Although there remain many issues to be resolved, and as the polymer nanoparticles are usually synthesized and utilized with water, we believe that this study is an important step forward for polymer nanoparticles to be used as a tough and sustainable material.

## CONCLUSIONS

In this study, we investigated the tear resistance of latex films formed from acrylic poly(ethyl acrylate-*co*-methyl methacrylate) nanoparticles cross-linked with a RC. In the tear tests, blunted crack propagation, in which the direction of crack propagation changes from horizontal to perpendicular with respect to the initial crack, was observed when the RC feed ratio exceeded 0.02 mol %. Analysis of the film width during the tear test revealed that the presence of RC in nanoparticles caused the blunted crack propagation. In addition, when the elongation rate of the tear test was varied, it was found that the blunted crack propagation occurred at low elongation rates. As the expression of the blunted crack propagation was found to depend on both the degree of rotaxane crosslinking within a nanoparticle and the elongation rate, it is plausible that the rotaxane crosslinking within a single nanoparticle is crucial for the formation of tough nanoparticle-based polymers. These results will help the development of new tough nanoparticle material and will find a variety of applications where nanoparticles are used, such as in coatings and adhesives.

## ASSOCIATED CONTENT

### Supporting Information

The Supporting Information is available free of charge at https://pubs.acs.org/doi/10.1021/acs.langmuir.3c01226.

Method for preparation of the latex films; AFM and TEM images of EM-R*X* nanoparticles; DSC curves for the EM nanoparticles; gel contents and the molecular weight of EM; photographs of the highly crosslinked EM-R0.4 film; crosslinker concentration-dependent tear resistance behaviors of the EM-R*X* films; tensile behavior of the unnotched films; elongation rate-dependent tear behavior of the EM-R*X* films (PDF)

Movie showing fracture behavior during tear tests for the EM film (MP4)

Movie showing fracture behavior during tear tests for the EM-R0.02 film (MP4)

## AUTHOR INFORMATION

### Corresponding Authors

**Toshikazu Takata** − *Department of Chemical Science and Engineering, Tokyo Institute of Technology, Yokohama, Kanagawa 226-8503, Japan; Graduate School of Advanced*



https://doi.org/10.1021/acs.langmuir.3c01226
*Langmuir* 2023, 39, 9262−9272

*Science and Engineering, Hiroshima University, Higashi-Hiroshima, Hiroshima 739-8527, Japan; orcid.org/0000-0002-4601-3443; Email: takatats@hiroshima-u.ac.jp*

**Daisuke Suzuki** − *Graduate School of Textile Science & Technology and Research Initiative for Supra-Materials, Interdisciplinary Cluster for Cutting Edge Research, Shinshu University, Ueda, Nagano 386-8567, Japan; orcid.org/0000-0003-0444-156X; Email: d_suzuki@shinshu-u.ac.jp*

### Authors

**Yuma Sasaki** − *Graduate School of Textile Science & Technology, Shinshu University, Ueda, Nagano 386-8567, Japan; orcid.org/0000-0002-6622-4299*

**Yuichiro Nishizawa** − *Graduate School of Textile Science & Technology, Shinshu University, Ueda, Nagano 386-8567, Japan*

**Takumi Watanabe** − *Graduate School of Textile Science & Technology, Shinshu University, Ueda, Nagano 386-8567, Japan; orcid.org/0000-0003-1471-4007*

**Takuma Kureha** − *Department of Frontier Materials Chemistry, Graduate School of Science and Technology, Hirosaki University, Hirosaki 036-8561, Japan; orcid.org/0000-0003-4680-6440*

**Kazuya Uenishi** − *Yokohama Rubber Co., Ltd., Hiratsuka, Kanagawa 254-8601, Japan*

**Kazuko Nakazono** − *Department of Chemical Science and Engineering, Tokyo Institute of Technology, Yokohama, Kanagawa 226-8503, Japan*

Complete contact information is available at: https://pubs.acs.org/10.1021/acs.langmuir.3c01226

### Author Contributions

Y.S., T.K., and D.S. wrote the draft of the manuscript. Y.S. conducted experiments related to the preparation and characterization of the nanoparticles and characterized the mechanical properties of the latex films. Y.N. and T.W. contributed to the research and discussion regarding the mechanical properties of the elastomers. T.K. contributed to the SAXS experiments. K.U. reviewed the entire manuscript. K.N. and T.T. provided the rotaxane crosslinker and reviewed the entire manuscript. D.S. designed and supervised the overall study.

### Notes

The authors declare no competing financial interest.

## ■ ACKNOWLEDGMENTS

D.S. acknowledges a CREST Grant-in Aid (JPMJCR21L2) from the Japan Science and Technology Agency (JST) and a Grant-in-Aid for A-STEP (JPMJTR20T6) from the Japan Science and Technology Agency (JST). Y.S. acknowledges a grant from the JST SPRING (Shinshu University) (JPMJSP2144) of the Japan Science and Technology Agency (JST). The X-ray diffraction analysis and experiments were performed on the BL03XU beamline at SPring-8 with the approval of the Japan Synchrotron Radiation Research Institute (proposals 2022A7201 and 2022B7251). The authors would like to thank Dr. Jun Sawada for preparing the rotaxane crosslinker used in this study.

## ■ REFERENCES

(1) Kawaguchi, H. Functional polymer microspheres. *Prog. Polym. Sci.* **2000**, *25*, 1171−1210.

(2) Zetterlund, P. B.; Kagawa, Y.; Okubo, M. Controlled/living radical polymerization in dispersed systems. *Chem. Rev.* **2008**, *108*, 3747−3794.

(3) Suzuki, D.; Horigome, K.; Kureha, T.; Matsui, S.; Watanabe, T. Polymeric hydrogel microspheres: design, synthesis, characterization, assembly and applications. *Polym. J.* **2017**, *49*, 695−702.

(4) Karg, M.; Pich, A.; Hellweg, T.; Hoare, T.; Lyon, L. A.; Crassous, J. J.; Suzuki, D.; Gumerov, R. A.; Schneider, S.; Potemkin, I. I.; Richtering, W. Nanogels and microgels: From model colloids to applications, recent developments, and future trends. *Langmuir* **2019**, *35*, 6231−6255.

(5) Minami, H. Preparation and morphology control of poly (ionic liquid) particles. *Langmuir* **2020**, *36*, 8668−8679.

(6) Holtz, J. H.; Asher, S. A. Polymerized colloidal crystal hydrogel films as intelligent chemical sensing materials. *Nature* **1997**, *389*, 829−832.

(7) Yue, M.; Hoshino, Y.; Miura, Y. Design rationale of thermally responsive microgel particle films that reversibly absorb large amounts of $CO_2$: fine tuning the pKa of ammonium ions in the particles. *Chem. Sci.* **2015**, *6*, 6112−6123.

(8) Kureha, T.; Nagase, Y.; Suzuki, D. High reusability of catalytically active gold nanoparticles immobilized in core−shell hydrogel microspheres. *ACS Omega* **2018**, *3*, 6158−6165.

(9) Fameau, A. L.; Fujii, S. Stimuli-responsive liquid foams: From design to applications. *Curr. Opin. Colloid Interface Sci.* **2020**, *50*, 101380.

(10) Suzuki, D.; McGrath, J. G.; Kawaguchi, H.; Lyon, L. A. Colloidal crystals of thermosensitive, core/shell hybrid microgels. *J. Phys. Chem. C* **2007**, *111*, 5667−5672.

(11) Okubo, T.; Suzuki, D.; Yamagata, T.; Horigome, K.; Shibata, K.; Tsuchida, A. Colloidal crystallization of thermosensitive gel spheres of poly (*N*-isopropylacrylamide) with low degree of cross-linking. *Colloid Polym. Sci.* **2011**, *289*, 1273−1281.

(12) Suzuki, D.; Yamagata, T.; Horigome, K.; Shibata, K.; Tsuchida, A.; Okubo, T. Colloidal crystallization of thermo-sensitive gel spheres of poly (*N*-isopropyl acrylamide). Influence of gel size. *Colloid Polym. Sci.* **2012**, *290*, 107−117.

(13) Kawamura, A.; Kohri, M.; Morimoto, G.; Nannichi, Y.; Taniguchi, T.; Kishikawa, K. Full-color biomimetic photonic materials with iridescent and non-iridescent structural colors. *Sci. Rep.* **2016**, *6*, 33984.

(14) Scott, P. J.; Kasprzak, C. R.; Feller, K. D.; Meenakshisundaram, V.; Williams, C. B.; Long, T. E. Light and latex: advances in the photochemistry of polymer colloids. *Polym. Chem.* **2020**, *11*, 3498−3524.

(15) Cho, E. C.; Kim, J. W.; Fernández-Nieves, A.; Weitz, D. A. Highly responsive hydrogel scaffolds formed by three-dimensional organization of microgel nanoparticles. *Nano Lett.* **2008**, *8*, 168−172.

(16) Suzuki, D.; Kobayashi, T.; Yoshida, R.; Hirai, T. Soft actuators of organized self-oscillating microgels. *Soft Matter* **2012**, *8*, 11447−11449.

(17) Keddie, J. L. Film formation of latex. *Mater. Sci. Eng., R* **1997**, *21*, 101−170.

(18) Winnik, M. A. Latex film formation. *Curr. Opin. Colloid Interface Sci.* **1997**, *2*, 192−199.

(19) Ito, T.; Katsura, C.; Sugimoto, H.; Nakanishi, E.; Inomata, K. Strain-responsive structural colored elastomers by fixing colloidal crystal assembly. *Langmuir* **2013**, *29*, 13951−13957.

(20) Jiang, S.; Van Dyk, A.; Maurice, A.; Bohling, J.; Fasano, D.; Brownell, S. Design colloidal particle morphology and self-assembly for coating applications. *Chem. Soc. Rev.* **2017**, *46*, 3792−3807.

(21) Kureha, T.; Hiroshige, S.; Matsui, S.; Suzuki, D. Water-immiscible bioinert coatings and film formation from aqueous dispersions of poly(2-methoxyethyl acrylate) microspheres. *Colloids Surf., B* **2017**, *155*, 166−172.

(22) Limousin, E.; Ballard, N.; Asua, J. M. Soft core−hard shell latex particles for mechanically strong VOC-free polymer films. *J. Appl. Polym. Sci.* **2019**, *136*, 47608.

(23) Jiménez, N.; Ballard, N.; Asua, J. M. Hydrogen bond-directed formation of stiff polymer films using naturally occurring polyphenols. *Macromolecules* **2019**, *52*, 9724−9734.
(24) Dron, S. M.; Paulis, M. Tracking hydroplasticization by DSC: Movement of water domains bound to poly (meth) acrylates during latex film formation. *Polymers* **2020**, *12*, 2500.
(25) Aguirre, M.; Ballard, N.; Gonzalez, E.; Hamzehlou, S.; Sardon, H.; Calderon, M.; Paulis, M.; Tomovska, R.; Dupin, D.; Bean, R. H.; Long, T. E.; Leiza, J. R.; Asua, J. M. Polymer Colloids: Current Challenges, Emerging Applications, and New Developments. *Macromolecules* **2023**, *56*, 2579−2607.
(26) Berce, P.; Skale, S.; Razboršek, T.; Slemnik, M. Influence of coalescing aids on the latex properties and film formation of waterborne coatings. *J. Appl. Polym. Sci.* **2017**, *134*, 45142.
(27) Ye, L.; Ma, G.; Zheng, S.; Huang, X.; Zhao, L.; Luo, H.; Liao, W. Facile fabrication of fluorine−silicon-containing poly (styrene−acrylate)/$SiO_2$ hydrophobic composites by combining physically mixing and sol−gel process. *JCT Res.* **2019**, *16*, 1243−1252.
(28) Li, C.; Cheng, W.; Yan, Z.; Ge, S.; Shao, Q.; Naik, N.; Pan, D.; Guo, Z. Soap-free styrene-acrylic/carbon nanotubes composite latex by in situ emulsion polymerization: Preparation, properties and characterizations. *Surf. Interfaces* **2021**, *25*, 101204.
(29) Limousin, E.; Ballard, N.; Asua, J. M. The influence of particle morphology on the structure and mechanical properties of films cast from hybrid latexes. *Prog. Org. Coat.* **2019**, *129*, 69−76.
(30) Cobaj, A.; Mehr, H. S.; Hu, Y.; Soucek, M. D. The influence of a non-isocyanate urethane monomer in the film formation and mechanical properties of homogeneous and core-shell latexes. *Polymer* **2021**, *214*, 123253.
(31) Taylor, J. W.; Winnik, M. A. Functional latex and thermoset latex films. *JCT Res.* **2004**, *1*, 163−190.
(32) Deplace, F.; Rabjohns, M. A.; Yamaguchi, T.; Foster, A. B.; Carelli, C.; Lei, C. H.; Ouzineb, K.; Keddie, J. L.; Lovell, P. A.; Creton, C. Deformation and adhesion of a periodic soft−soft nanocomposite designed with structured polymer colloid particles. *Soft Matter* **2009**, *5*, 1440−1447.
(33) Lesage de la Haye, J.; Martin-Fabiani, I.; Schulz, M.; Keddie, J. L.; D'agosto, F.; Lansalot, M. Hydrophilic MacroRAFT-mediated emulsion polymerization: Synthesis of latexes for cross-linked and surfactant-free films. *Macromolecules* **2017**, *50*, 9315−9328.
(34) Xu, K.; Fan, B.; Putera, K.; Wawryk, M.; Wan, J.; Peng, B.; Banaszak Holl, M. M.; Patti, A. F.; Thang, S. H. Nanoparticle surface cross-linking: A universal strategy to enhance the mechanical properties of latex films. *Macromolecules* **2022**, *55*, 5301−5313.
(35) Chen, Y.; Jones, S. T.; Hancox, I.; Beanland, R.; Tunnah, E. J.; Bon, S. A. Multiple hydrogen-bond array reinforced cellular polymer films from colloidal crystalline assemblies of soft latex particles. *ACS Macro Lett.* **2012**, *1*, 603−608.
(36) Wu, Y.; Wang, Y.; Wan, X.; Gao, C.; Liu, Y. Chitosan strengthened and multiple hydrogen bonds crosslinked styrene-acrylate coatings as conductive substrate with excellent mechanical performance. *Prog. Org. Coat.* **2022**, *164*, 106705.
(37) Hiroshige, S.; Kureha, T.; Aoki, D.; Sawada, J.; Aoki, D.; Takata, T.; Suzuki, D. Formation of tough films by evaporation of water from dispersions of elastomer microspheres crosslinked with rotaxane supramolecules. *Chem.—Eur. J.* **2017**, *23*, 8405−8408.
(38) Hiroshige, S.; Sawada, J.; Aoki, D.; Takata, T.; Suzuki, D. Investigation of mechanical properties of latex films prepared from poly (butyl acrylate-*co*-methyl methacrylate) microspheres crosslinked with rotaxane. *J. Soc. Rheol., Jpn.* **2019**, *47*, 051−054.
(39) Kureha, T.; Hiroshige, S.; Suzuki, D.; Sawada, J.; Aoki, D.; Takata, T.; Shibayama, M. Quantification for the mixing of polymers on microspheres in waterborne latex films. *Langmuir* **2020**, *36*, 4855−4862.
(40) Okumura, Y.; Ito, K. The polyrotaxane gel: a topological gel by figure-of-eight cross-links. *Adv. Mater.* **2001**, *13*, 485−487.
(41) Sawada, J.; Aoki, D.; Uchida, S.; Otsuka, H.; Takata, T. Synthesis of vinylic macromolecular rotaxane cross-linkers endowing network polymers with toughness. *ACS Macro Lett.* **2015**, *4*, 598−601.
(42) Liu, C.; Kadono, H.; Mayumi, K.; Kato, K.; Yokoyama, H.; Ito, K. Unusual fracture behavior of slide-ring gels with movable cross-links. *ACS Macro Lett.* **2017**, *6*, 1409−1413.
(43) Gotoh, H.; Liu, C.; Imran, A. B.; Hara, M.; Seki, T.; Mayumi, K.; Ito, K.; Takeoka, Y. Optically transparent, high-toughness elastomer using a polyrotaxane cross-linker as a molecular pulley. *Sci. Adv.* **2018**, *4*, No. eaat7629.
(44) Lake, G. J.; Thomas, A. G. The strength of highly elastic materials. *Proc. Roy. Soc. Lond. Math. Phys. Sci.* **1967**, *300*, 108−119.
(45) Tsunoda, K.; Busfield, J. J. C.; Davies, C. K. L.; Thomas, A. G. Effect of materials variables on the tear behaviour of a non-crystallising elastomer. *J. Mater. Sci.* **2000**, *35*, 5187−5198.
(46) Yang, W.; Sherman, V. R.; Gludovatz, B.; Schaible, E.; Stewart, P.; Ritchie, R. O.; Meyers, M. A. On the tear resistance of skin. *Nat. Commun.* **2015**, *6*, 6649.
(47) Osumi, R.; Yasui, T.; Tanaka, R.; Mai, T. T.; Takagi, H.; Shimizu, N.; Tsunoda, K.; Sakurai, S.; Urayama, K. Impact of strain-induced crystallization on fast crack growth in stretched *cis*-1, 4-polyisoprene rubber. *ACS Macro Lett.* **2022**, *11*, 747−752.
(48) Sawada, J.; Aoki, D.; Kuzume, M.; Nakazono, K.; Otsuka, H.; Takata, T. A vinylic rotaxane cross-linker for toughened network polymers from the radical polymerization of vinyl monomers. *Polym. Chem.* **2017**, *8*, 1878−1881.
(49) Antonietti, M.; Landfester, K. Polyreactions in miniemulsions. *Prog. Polym. Sci.* **2002**, *27*, 689−757.
(50) Mayumi, K.; Guo, J.; Narita, T.; Hui, C. Y.; Creton, C. Fracture of dual crosslink gels with permanent and transient crosslinks. *Extreme Mech. Lett.* **2016**, *6*, 52−59.
(51) Hashimoto, T.; Nagatoshi, K.; Todo, A.; Hasegawa, H.; Kawai, H. Domain-Boundary Structure of Styrene-Isoprene Block Copolymer Films Cast from Toluene Solutions. *Macromolecules* **1974**, *7*, 364−373.
(52) Perrin, P.; Prudhomme, R. E. SAXS Measurements of Interfacial Thickness in Amorphous Polymer Blends Containing a Diblock Copolymer. *Macromolecules* **1994**, *27*, 1852−1860.
(53) Kim, J.-E.; Zin, W.-C.; Ahn, J.-H. Interfacial change on morphological transitions in styrene−isoprene diblock copolymer. *Eur. Polym. J.* **2009**, *45*, 2450−2454.
(54) Hiroshige, S.; Minato, H.; Nishizawa, Y.; Sasaki, Y.; Kureha, T.; Shibayama, M.; Uenishi, K.; Takata, T.; Suzuki, D. Temperature-dependent relationship between the structure and mechanical strength of volatile organic compound-free latex films prepared from poly (butyl acrylate-*co*-methyl methacrylate) microspheres. *Polym. J.* **2021**, *53*, 345−353.
(55) Watanabe, T.; Minato, H.; Sasaki, Y.; Hiroshige, S.; Suzuki, H.; Matsuki, N.; Sano, K.; Wakiya, T.; Nishizawa, Y.; Uchihashi, T.; Kureha, T.; Shibayama, M.; Takata, T.; Suzuki, D. Closed-loop recycling of microparticle-based polymers. *Green Chem.* **2023**, *25*, 3418−3424.
(56) Ruland, W. Small-angle scattering of two-phase systems: determination and significance of systematic deviations from Porod's law. *J. Appl. Crystallogr.* **1971**, *4*, 70−73.
(57) Kuo, S. W.; Kao, H. C.; Chang, F. C. Thermal behavior and specific interaction in high glass transition temperature PMMA copolymer. *Polymer* **2003**, *44*, 6873−6882.
(58) Sasaki, Y.; Hiroshige, S.; Takizawa, M.; Nishizawa, Y.; Uchihashi, T.; Minato, H.; Suzuki, D. Non-close-packed arrangement of soft elastomer microspheres on solid substrates. *RSC Adv.* **2021**, *11*, 14562−14567.
(59) Kan, C. Y.; Liu, D. S.; Kong, X. Z.; Zhu, X. L. Study on the preparation and properties of styrene−butyl acrylate−silicone copolymer latices. *J. Appl. Polym. Sci.* **2001**, *82*, 3194−3200.
(60) Kato, K.; Ikeda, Y.; Ito, K. Direct determination of cross-link density and its correlation with the elastic modulus of a gel with slidable cross-links. *ACS Macro Lett.* **2019**, *8*, 700−704.
(61) Yasuda, Y.; Masumoto, T.; Mayumi, K.; Toda, M.; Yokoyama, H.; Morita, H.; Ito, K. Molecular dynamics simulation and theoretical


https://doi.org/10.1021/acs.langmuir.3c01226
*Langmuir* 2023, 39, 9262−9272

model of elasticity in slide-ring gels. *ACS Macro Lett.* **2020**, *9*, 1280−1285.
(62) Konko, I.; Guriyanova, S.; Boyko, V.; Sun, L.; Liu, D.; Reck, B.; Men, Y. Role of the hydrophilic latex particle surface in water diffusion into films from waterborne polymer colloids. *Langmuir* **2019**, *35*, 6075−6088.
(63) Aradian, A.; Raphael, E.; De Gennes, P. G. A scaling theory of the competition between interdiffusion and cross-linking at polymer interfaces. *Macromolecules* **2002**, *35*, 4036−4043.
(64) Yoo, J. N.; Sperling, L. H.; Glinka, C. J.; Klein, A. Characterization of film formation from polystyrene latex particles via SANS [small-angle neutron scattering]. 1. Moderate molecular weight. *Macromolecules* **1990**, *23*, 3962−3967.
(65) Yoo, J. N.; Sperling, L. H.; Glinka, C. J.; Klein, A. Characterization of Film Formation from Polystyrene Latex Particles via SANS. 2. High Molecular Weight. *Macromolecules* **1991**, *24*, 2868−2876.
(66) Kim, K. D.; Sperling, L. H.; Klein, A.; Hammouda, B. Reptation time, temperature, and cosurfactant effects on the molecular interdiffusion rate during polystyrene latex film formation. *Macromolecules* **1994**, *27*, 6841−6850.
(67) Luo, F.; Sun, T. L.; Nakajima, T.; Kurokawa, T.; Zhao, Y.; Ihsan, A. B.; Guo, H. L.; Li, X. F.; Gong, J. P. Crack blunting and advancing behaviors of tough and self-healing polyampholyte hydrogel. *Macromolecules* **2014**, *47*, 6037−6046.
(68) Liu, C.; Yokoyama, H.; Mayumi, K.; Ito, K. Crack velocity dependent toughness of polyrotaxane networks: The sliding dynamics of rings on polymer under stretching. *Mech. Mater.* **2021**, *156*, 103784.
(69) Greensmith, H. W. Rupture of rubber. IV. Tear properties of vulcanizates containing carbon black. *J. Polym. Sci.* **1956**, *21*, 175−187.
(70) Brüning, K.; Schneider, K.; Roth, S. V.; Heinrich, G. Strain-induced crystallization around a crack tip in natural rubber under dynamic load. *Polymer* **2013**, *54*, 6200−6205.
(71) Kazem, N.; Bartlett, M. D.; Majidi, C. Extreme toughening of soft materials with liquid metal. *Adv. Mater.* **2018**, *30*, 1706594.
(72) King, D. R.; Sun, T. L.; Huang, Y.; Kurokawa, T.; Nonoyama, T.; Crosby, A. J.; Gong, J. P. Extremely tough composites from fabric reinforced polyampholyte hydrogels. *Mater. Horiz.* **2015**, *2*, 584−591.
(73) Wang, Z.; Xiang, C.; Yao, X.; Le Floch, P.; Mendez, J.; Suo, Z. Stretchable materials of high toughness and low hysteresis. *Proc. Natl. Acad. Sci. U.S.A.* **2019**, *116*, 5967−5972.
(74) Guo, H.; Sanson, N.; Hourdet, D.; Marcellan, A. Thermoresponsive toughening with crack bifurcation in phase-separated hydrogels under isochoric conditions. *Adv. Mater.* **2016**, *28*, 5857−5864.
(75) Zhuo, Y.; Xia, Z.; Qi, Y.; Sumigawa, T.; Wu, J.; Šesták, P.; Lu, Y.; Håkonsen, V.; Li, T.; Wang, F.; Chen, W.; Xiao, S.; Long, R.; Kitamura, T.; Li, L.; He, J.; Zhang, Z. Simultaneously toughening and stiffening elastomers with octuple hydrogen bonding. *Adv. Mater.* **2021**, *33*, 2008523.
(76) Lee, S.; Pharr, M. Sideways and stable crack propagation in a silicone elastomer. *Proc. Natl. Acad. Sci. U.S.A.* **2019**, *116*, 9251−9256.


https://doi.org/10.1021/acs.langmuir.3c01226
*Langmuir* 2023, 39, 9262−9272